Supporting Information for:

Pentaarylbiimidazole, PABI: An Easily Synthesized Fast Photochromic Molecule with Superior Durability

Hiroaki Yamashita[†] *and Jiro Abe*[*,†,‡]

[†]*Department of Chemistry, School of Science and Engineering, Aoyama Gakuin University, 5-10-1 Fuchinobe, Chuo-ku, Sagamihara, Kanagawa 252-5258, Japan*

[‡]*CREST, Japan Science and Technology Agency (JST), K's Gobancho, 7 Gobancho, Chiyoda-ku, Tokyo 102-0076, Japan.*

E-mail: *jiro_abe@chem.aoyama.ac.jp*

CONTENTS

1. Synthesis

Scheme S1.

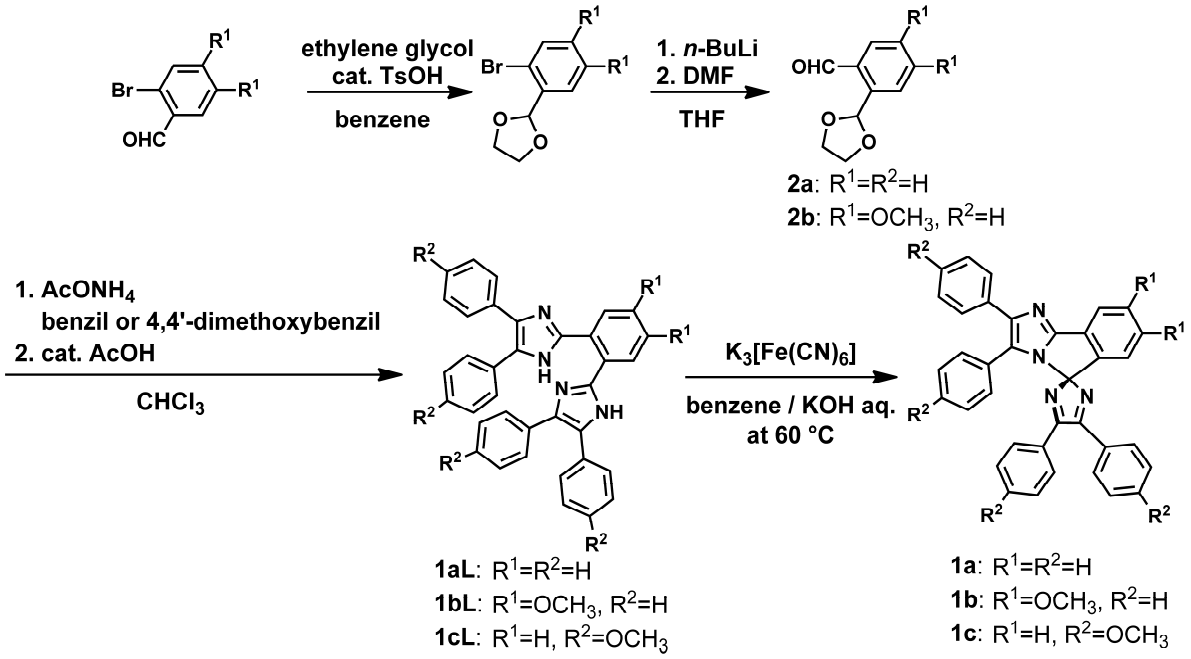

All reactions were monitored by thin-layer chromatography carried out on 0.2 mm E. Merck silica gel plates (60F-254). Column chromatography was performed on silica gel (Wakogel® C-300). ^{1}H NMR spectra were recorded at 400 MHz on a Bruker AVANCE III 400 NanoBay. DMSO-d_6 and $CDCl_3$ were used as deuterated solvent. ESI–TOF–MS spectra were recorded on a Bruker micrOTOF II-AGA1. All glassware was washed with distilled water and dried. Unless otherwise noted, all reagents and reaction solvents were purchased from TCI, Wako Co. Ltd., Aldrich Chemical Co., Inc., and ACROS Organics and were used without further purification.

2-(1,3-dioxolan-2-yl)benzaldehyde (2a) and **2-(1,3-dioxolan-2-yl)-4,5-dimethoxybenzaldehyde (2b)** were prepared according to a literature procedure.[S1]

1,2-bis(4,5-diphenyl-1*H*-imidazol-2-yl)benzene (1aL)

Compound **2a** (412 mg, 2.31 mmol), benzil (513 mg, 2.44 mmol), and ammonium acetate (747 mg, 9.69 mmol) were stirred at 110 °C in $CHCl_3$ (8 mL) in a sealed tube for 18 h. Then, acetic acid (1 mL) was added and the reaction mixture was stirred at 110 °C in a sealed tube for 24 h. The reaction mixture was cooled to room temperature and neutralized by aqueous NH_3. The organic extract was washed with water and dried over $MgSO_4$. After removal of the solvents, the crude product was purified by recrystallized from $CHCl_3$/hexane to give **1aL** as colorless crystals, 596 mg (1.16 mmol, 50%). ^{1}H NMR (400 MHz, DMSO-d_6) δ: 14.08 (s, 2H), 8.19–8.17 (m, 2H), 7.61–7.59 (m, 2H), 7.32 (s, 3H), 7.55–7.41 (m, 10H), 7.30–7.28 (m, 12H).

2,3,4',5'-tetraphenylspiro[imidazo[2,1-a]isoindole-5,2'-imidazole] (1a)

A solution of potassium ferricyanide (754 mg, 2.26 mmol), KOH (200 mg, 3.56 mmol) in water (20 mL)

was added to a suspension of **1aL** (38.7 mg, 0.0752 mmol) in benzene (5 mL). After stirring for 2 h at 60 °C, the resultant mixture was then extracted with benzene and the organic extract was washed with water and dried over MgSO4. After removal of the solvents, the residual powder was purified by recrystallized from CH_2Cl_2/hexane to give **1a** as yellow crystals, (34.7 mg, yield: 90%). ^{1}H NMR (400 MHz, $CDCl_3$) δ: 8.03 (d, *J*=7.5 Hz, 1H), 7.57 (d, *J*=7.1 Hz, 2H), 7.53–7.49 (m, 3H), 7.38–7.35 (m, 4H), 7.30–7.28 (m, 7H)7.25–7.10 (m, 6H), 6.84 (d, *J*=6.8 Hz, 1H); HRMS (ESI-TOF) calculated for $C_{36}H_{25}N_4$ $[M+H]^+$: 513.2074, found: 513.2075.

2,2'-(4,5-dimethoxy-1,2-phenylene)bis(4,5-diphenyl-1H-imidazole) (1bL)

Compound **2b** (116 mg, 0.487 mmol), benzil (109 mg, 0.518 mmol), and ammonium acetate (300 mg, 3.89 mmol) were stirred at 110 °C in $CHCl_3$ (3 mL) in a sealed tube for 18 h. Then, acetic acid (1 mL) was added and the reaction mixture was stirred at 110 °C in a sealed tube for 24 h. The reaction mixture was cooled to room temperature and neutralized by aqueous NH_3. The organic extract was washed with water and dried over $MgSO_4$. After removal of the solvents, the crude product was purified by recrystallized from $CHCl_3$/hexane to give **1bL** as colorless crystals, 138 mg (0.240 mmol, 49%). ^{1}H NMR (400 MHz, DMSO-d_6) δ: 14.10 (s, 2H), 7.70 (s, 2H), 7.49–7.47 (m, 4H), 7.39–7.38 (m, 4H), 7.29–7.27 (m, 12H), 3.93 (s, 6H).

7,8-dimethoxy-2,3,4',5'-tetraphenylspiro[imidazo[2,1-a]isoindole-5,2'-imidazole] (1b)

A solution of potassium ferricyanide (367 mg, 1.11 mmol), KOH (203 mg, 3.62 mmol) in water (20 mL) was added to a suspension of **1bL** (54.8 mg, 0.0954 mmol) in benzene (10 mL). After stirring for 2 h at 60 °C, the resultant mixture was then extracted with benzene and the organic extract was washed with water and dried over $MgSO_4$. After removal of the solvents, the residual powder was purified by silica gel column chromatography (hexane/AcOEt =1/1) to give **1b** as yellow solid, (44.0 mg, yield: 81%). ^{1}H NMR (400 MHz, $CDCl_3$) δ: 7.59 (s, 1H), 7.56–7.50 (m, 4H), 7.39–7.35 (m, 4H), 7.31–7.28 (m, 6H), 7.23–7.08 (m, 6H), 6.31 (s, 1H), 4.01 (s, 3H), 3.81 (s, 3H); HRMS (ESI-TOF) calculated for $C_{38}H_{29}N_4O_2$ $[M+H]^+$: 573.2285, found: 573.2290.

1,2-bis(4,5-bis(4-methoxyphenyl)-1H-imidazol-2-yl)benzene (1cL)

Compound **2a** (501 mg, 2.81 mmol), 4,4'-dimethoxybenzil (1.60 g, 5.92 mmol), and ammonium acetate (1.21 g, 15.7 mmol) were stirred at 110 °C in $CHCl_3$ (8 mL) in a sealed tube for 24 h. Then, acetic acid (1 mL) was added and the reaction mixture was stirred at 110 °C in a sealed tube for 24 h. The reaction mixture was cooled to room temperature and neutralized by aqueous NH_3. The organic extract was washed with water and dried over $MgSO_4$. After removal of the solvents, the crude product was purified by silica gel column chromatography (hexane/AcOEt =1/1) to give **1cL** as yellow solid, 710 mg (1.10 mmol, 39%). ^{1}H NMR (400 MHz, DMSO-d_6) δ: 14.08 (s, 2H), 8.17–8.15 (m, 2H), 7.57–7.54 (m, 2H), 7.35 (s, 8H), 6.86 (d, *J*=8.8 Hz, 8H), 3.77 (s, 12H).

2,3,4',5'-tetrakis(4-methoxyphenyl)spiro[imidazo[2,1-a]isoindole-5,2'-imidazole] (1c)

A solution of potassium ferricyanide (1.34 g, 4.07 mmol), KOH (406 mg, 7.24 mmol) in water (20 mL) was added to a suspension of **1cL** (334 mg, 0.542 mmol) in benzene (10 mL). After stirring for 2 h at 60 °C, the resultant mixture was then extracted with benzene and the organic extract was washed with water and dried over $MgSO_4$. After removal of the solvents, the residual powder was purified by silica gel column chromatography (hexane/AcOEt =1/1) to give **1c** as yellow solid, (310 mg, yield: 90%). ^{1}H NMR (400 MHz, $CDCl_3$) δ: 7.98 (d, *J*=7.6 Hz, 1H), 7.67–7.63 (m, 1H), 7.53 (d, *J*=8.9 Hz, 2H), 7.44–7.41 (m, 1H), 7.30 (d, *J*=5.1 Hz, 5H), 7.26 (d, *J*=7.7 Hz, 4H), 7.16(d, *J*=8.7 Hz, 2H), 7.06 (d, *J*=8.9 Hz, 4H), 6.90 (d, *J*=8.9 Hz, 2H), 6.75 (d, *J*=8.7 Hz, 2H), 3.88 (s, 6H) 3.77 (s, 3H), 3.70 (s, 3H); HRMS (ESI-TOF) calculated for $C_{40}H_{33}N_4O_4$ $[M+H]^+$: 633.2496, found: 633.2503.

2. ^{1}H NMR Spectra

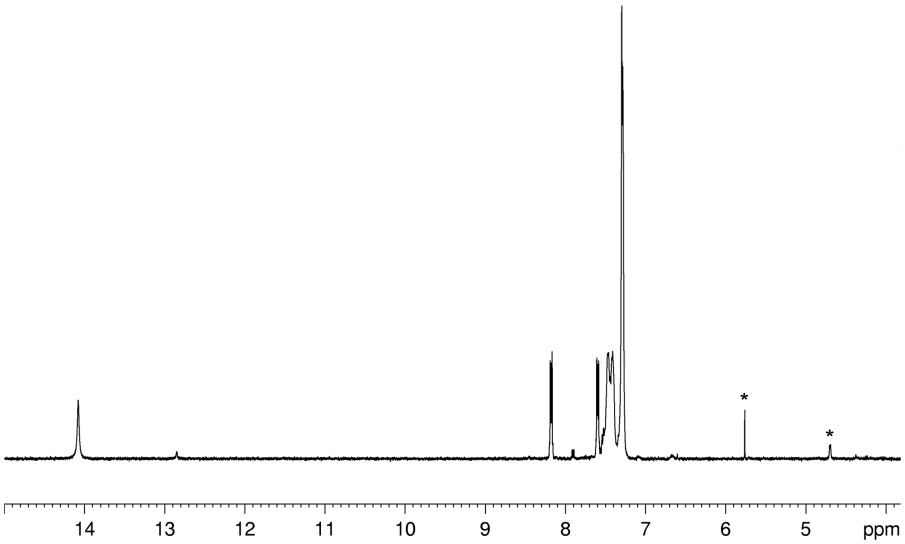

Figure S1. ^{1}H NMR spectrum of **1aL** in DMSO-d_6 (* solvent peaks).

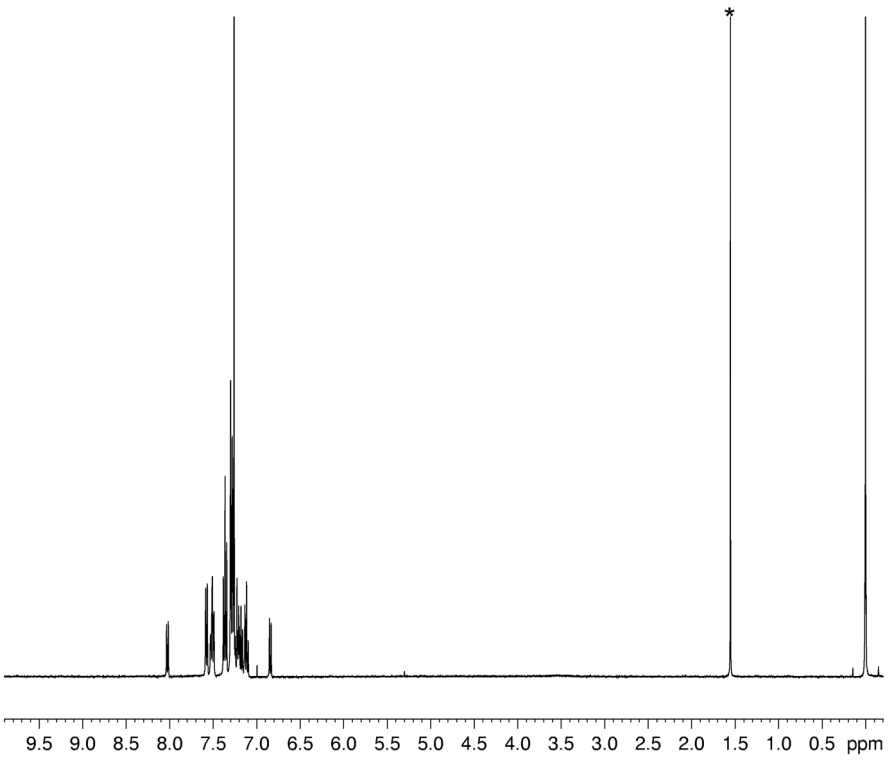

Figure S2. ^{1}H NMR spectrum of **1a** in $CDCl_3$ (* solvent peaks).

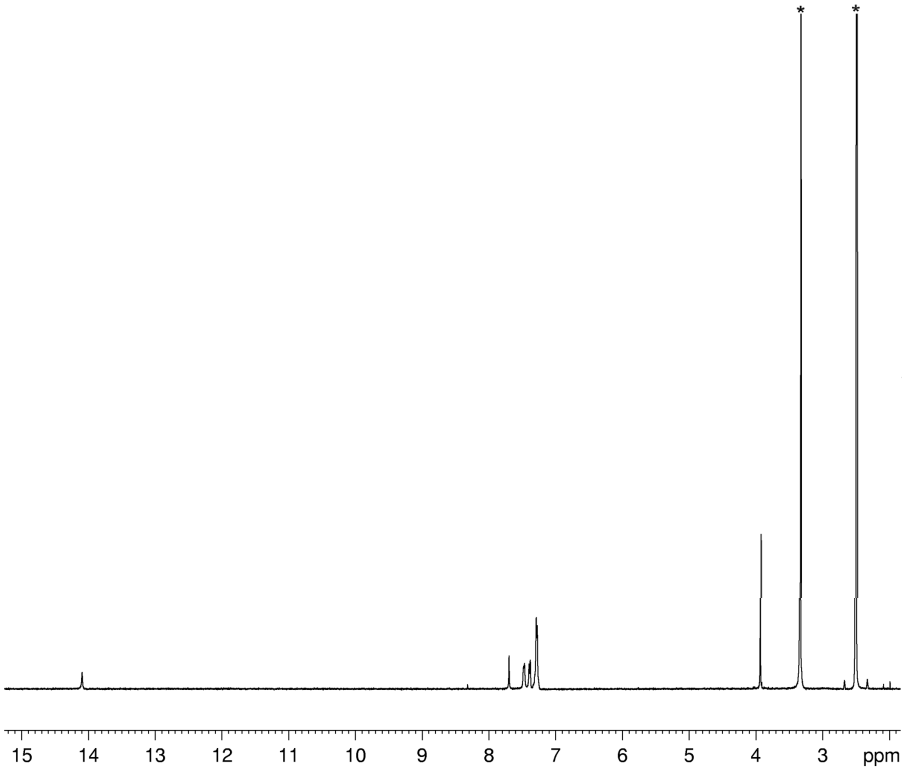

Figure S3. ^{1}H NMR spectrum of **1bL** in DMSO-d_6 (* solvent peaks).

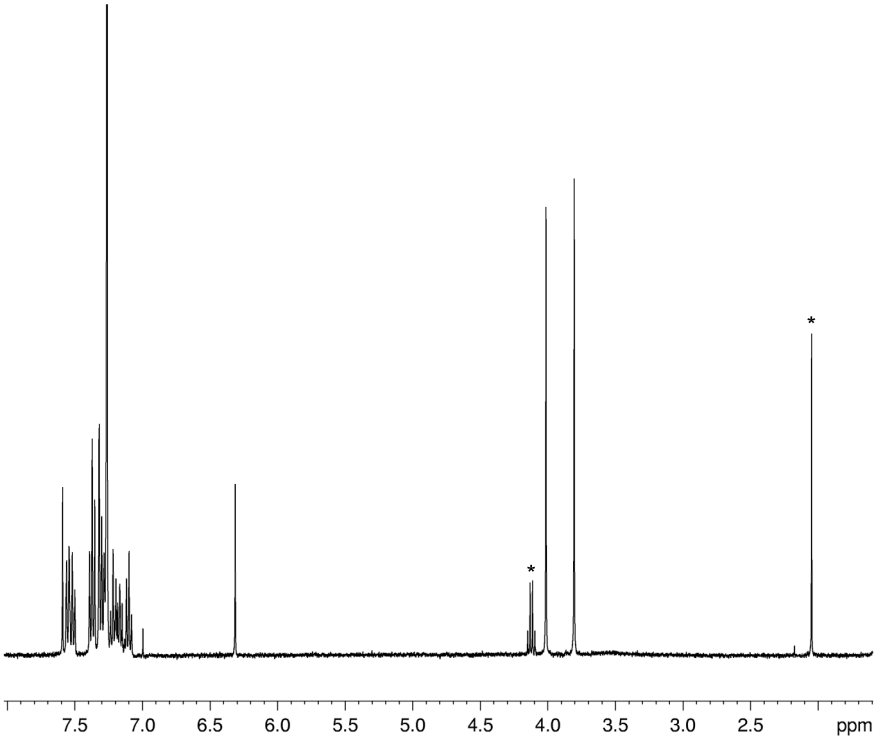

Figure S4. ^{1}H NMR spectrum of **1b** in $CDCl_3$ (* solvent peaks).

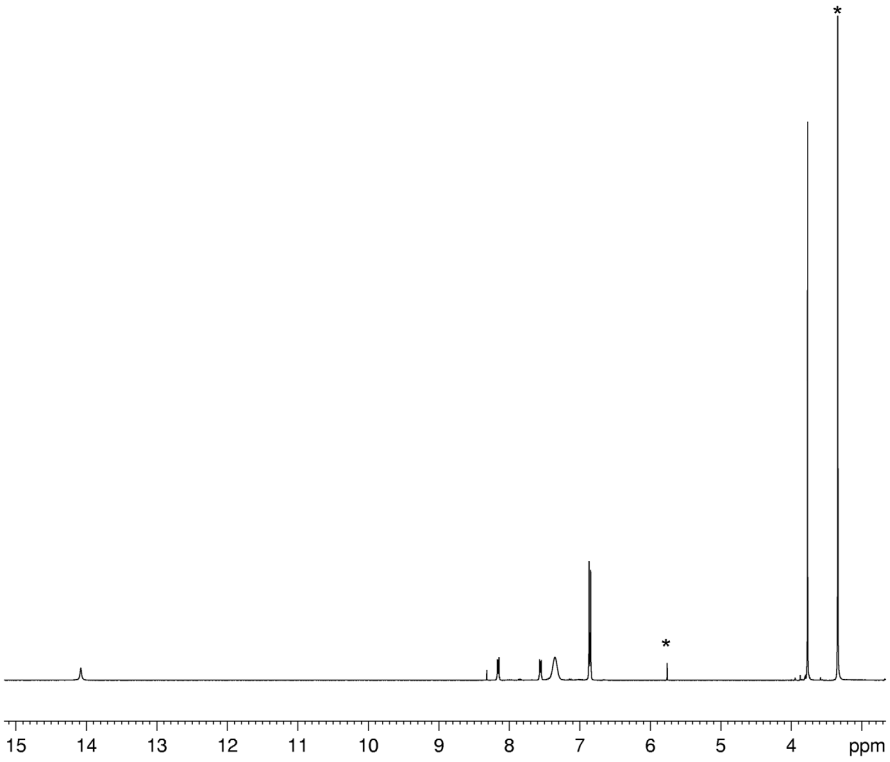

Figure S5. ^{1}H NMR spectrum of **1cL** in DMSO-d_6 (* solvent peaks).

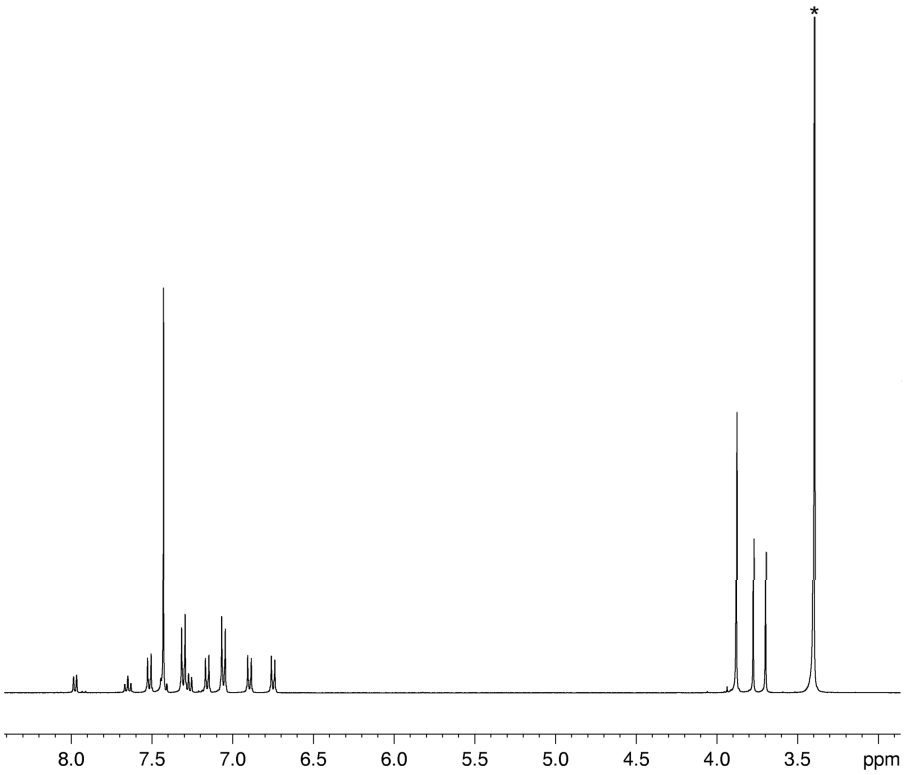

Figure S6. ^{1}H NMR spectrum of **1c** in $CDCl_3$ (* solvent peaks).

3. HR-ESI-TOF-MS Spectra

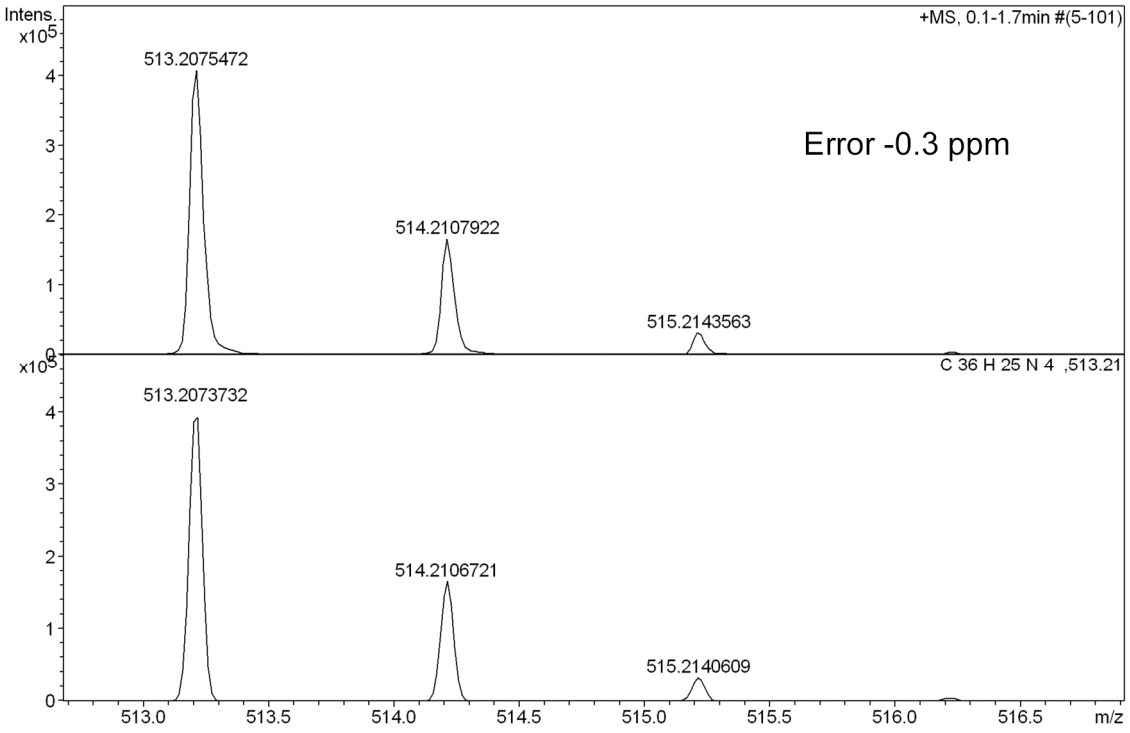

Figure S7. HR-ESI-TOF-MS of **1a**.

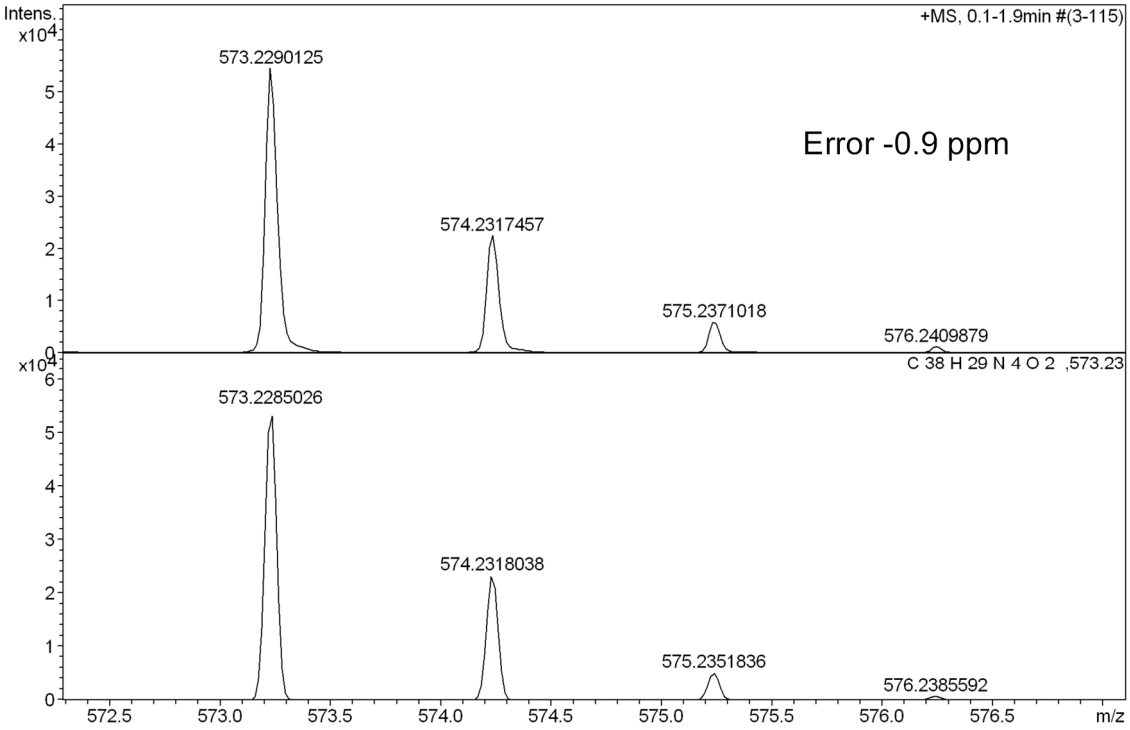

Figure S8. HR-ESI-TOF-MS of **1b**.

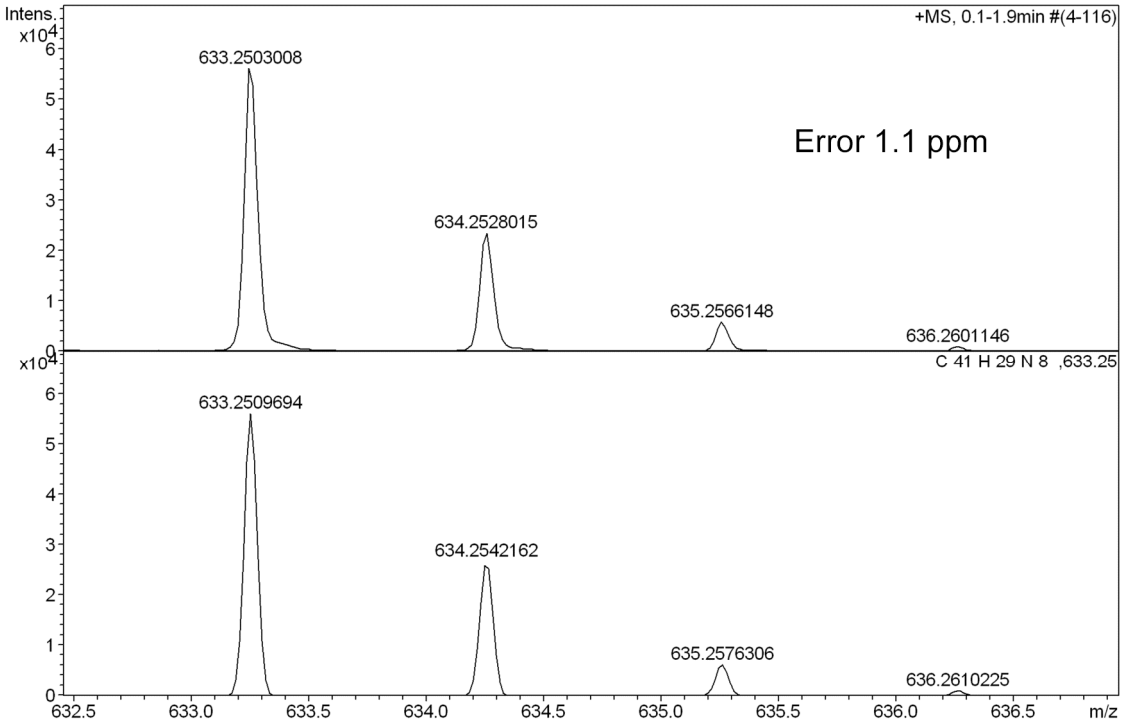

Figure S9. HR-ESI-TOF-MS of **1c**.

4. HPLC Chromatograms

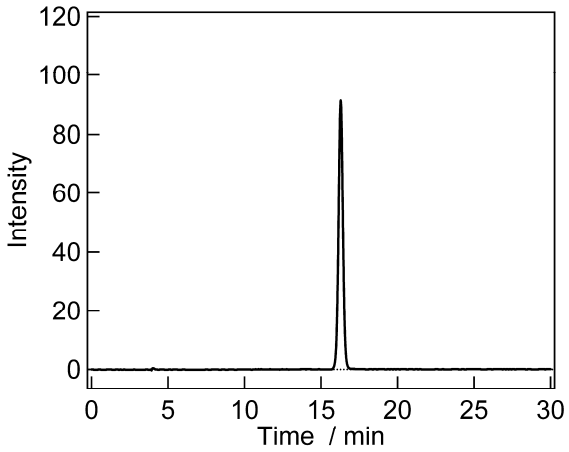

Figure S10. HPLC chromatogram of **1a**; 99% purity. HPLC analysis was performed using a reverse phase analytical column (Mightysil RP18, 25cm×4.6mm, 5μm particle) from Kanto Chemical Industries, equipped with a UV detector; the mobile phase was CH_3CN/H_2O = 7/3 with a flow rate of 1.0 mL/min (range; 0.01, inject volume; 3μL, detection wavelength; 254 nm).

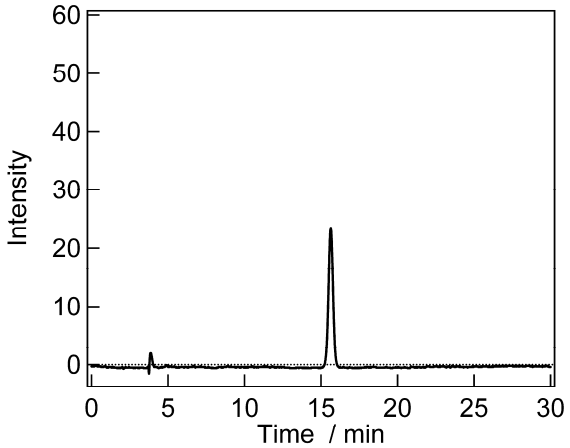

Figure S11. HPLC chromatogram of **1a**; 99% purity. HPLC analysis was performed using a reverse phase analytical column (Mightysil RP18, 25cm×4.6mm, 5μm particle) from Kanto Chemical Industries, equipped with a UV detector; the mobile phase was CH_3CN/H_2O = 7/3 with a flow rate of 1.0 mL/min (range; 0.0025, inject volume; 3μL, detection wavelength; 355 nm).

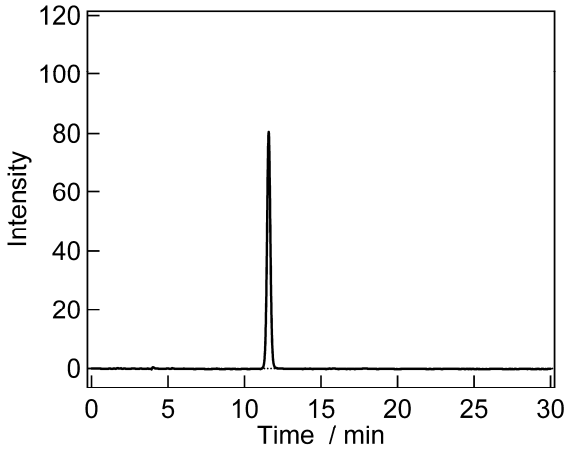

Figure S12. HPLC chromatogram of **1b**; 99% purity. HPLC analysis was performed using a reverse phase analytical column (Mightysil RP18, 25cm×4.6mm, 5μm particle) from Kanto Chemical Industries, equipped with a UV detector; the mobile phase was CH_3CN/H_2O = 7/3 with a flow rate of 1.0 mL/min (range; 0.01, inject volume; 3μL, detection wavelength; 254 nm).

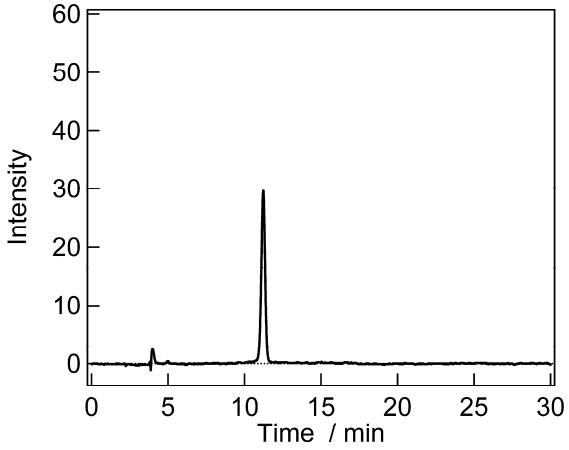

Figure S13. HPLC chromatogram of **1b**; 99% purity. HPLC analysis was performed using a reverse phase analytical column (Mightysil RP18, 25cm×4.6mm, 5μm particle) from Kanto Chemical Industries, equipped with a UV detector; the mobile phase was CH_3CN/H_2O = 7/3 with a flow rate of 1.0 mL/min (range; 0.0025, inject volume; 3μL, detection wavelength; 355 nm).

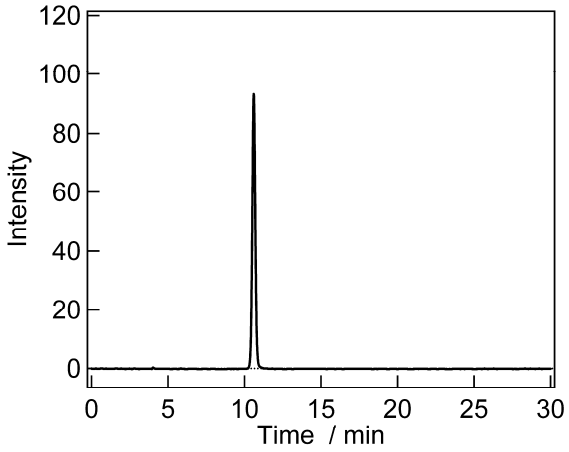

Figure S14. HPLC chromatogram of **1c**; 99% purity. HPLC analysis was performed using a reverse phase analytical column (Mightysil RP18, 25cm×4.6mm, 5μm particle) from Kanto Chemical Industries, equipped with a UV detector; the mobile phase was CH_3CN/H_2O = 7/3 with a flow rate of 1.0 mL/min (range; 0.01, inject volume; 3μL, detection wavelength; 254 nm).

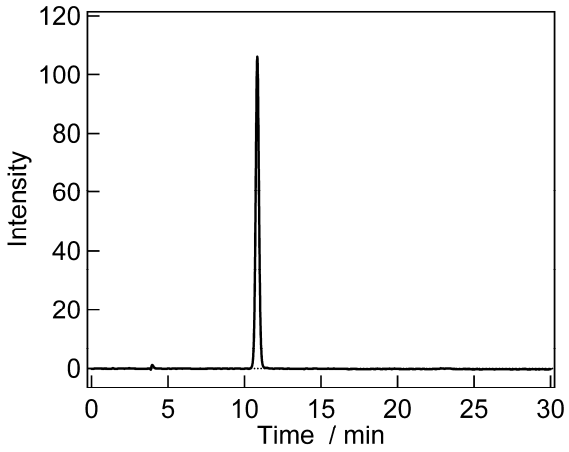

Figure S15. HPLC chromatogram of **1c**; 99% purity. HPLC analysis was performed using a reverse phase analytical column (Mightysil RP18, 25cm×4.6mm, 5μm particle) from Kanto Chemical Industries, equipped with a UV detector; the mobile phase was CH_3CN/H_2O = 7/3 with a flow rate of 1.0 mL/min (range; 0.005, inject volume; 3μL, detection wavelength; 355 nm).

5. X-ray Crystallographic Analysis

The diffraction data of the single crystals were collected on the Bruker APEX II CCD area detector (Mo Kα, λ = 0.71073 nm). The data refinement was carried out by the Bruker APEXII software package with SHELXT program.[S2,S3] All non-hydrogen atoms were anisotropically refined.

Table S1. Crystallographic parameters of **1aL**.

Identification code	**1aL**
Empirical formula	$C_{36}H_{26}N_4$
Formula weight	514.61
Temperature	90(0) K
Wavelength	0.71073 Å
Crystal system	triclinic
Space group	P -1
Unit cell dimensions	a = 9.0514(11) Å
	b = 12.8065(11) Å
	c = 12.8890(15) Å
Volume	1350.9(3) $Å^3$
Z	2
Density (calculated)	1.260 Mg/m^3
Absorption coefficient	0.075 mm^{-1}
F(000)	536
Theta range for data collection	1.68 to 27.50
Index ranges	-11<=h<=7, -16<=k<=16, -13<=l<=16
Reflections collected	7702
Independent reflections	5844 [R(int) = 0.0181]
Absorption correction	Empirical
Refinement method	Full-matrix least-squares on F^2
Data / restraints / parameters	5844 / 0 / 370
Goodness-of-fit on F^2	1.322
Final R indices [I>2sigma(I)]	R1 = 0.0459, wR2 = 0.0617
R indices (all data)	R1 = 0.0721, wR2 = 0.0660
Largest diff. peak and hole	0.241 and -0.250 $eÅ^{-3}$

Table S2. Crystallographic parameters of **1a**.

Identification code	**1a**
Empirical formula	$C_{36}H_{24}N_4$
Formula weight	512.59
Temperature	90(0) K
Wavelength	0.71073 Å
Crystal system	orthorhombic
Space group	P n a 21
Unit cell dimensions	a = 15.8279(16) Å
	b = 13.8209(7) Å
	c = 14.2201(7) Å
Volume	2693.1(5) $Å^3$
Z	4
Density (calculated)	1.264 Mg/m^3
Absorption coefficient	0.075 mm^{-1}
F(000)	1072
Theta range for data collection	1.89 to 25.95°
Index ranges	-19<=h<=19, -17<=k<=18, -14<=l<=9
Reflections collected	13236
Independent reflections	4290 [R(int) = 0.0450]
Absorption correction	Empirical
Refinement method	Full-matrix least-squares on F^2
Data / restraints / parameters	4290 / 1 / 362
Goodness-of-fit on F^2	1.034
Final R indices [I>2sigma(I)]	R1 = 0.0396, wR2 = 0.0834
R indices (all data)	R1 = 0.0517, wR2 = 0.0890
Largest diff. peak and hole	0.172 and -0.189 $eÅ^{-3}$

6. Experimental Detail for Laser Flash Photolysis measurements

The laser flash photolysis experiments were carried out with a TSP-1000 time resolved spectrophotometer (Unisoku). A 10 Hz Q-switched Nd:YAG (Continuum Minilite II) laser with the third harmonic at 355 nm (ca. 4 mJ per 5 ns pulse) was employed for the excitation light. The probe beam from a halogen lamp (OSRAM HLX64623) was guided with an optical fiber scope to be arranged in an orientation perpendicular to the exciting laser beam. The probe beam was monitored with a photomultiplier tube (Hamamatsu R2949) through a spectrometer (Unisoku MD200) for the decay profile of the colored species.

7. Kinetics for the Thermal Back-Reaction

Table S3. First-order rate constants for the thermal back-reaction of **1aR**.

T / K	k / s^{-1}
278	1.1×10^5
283	1.5×10^5
288	2.2×10^5
293	2.8×10^5
298	3.5×10^5
303	4.4×10^5
308	5.6×10^5
313	7.4×10^5

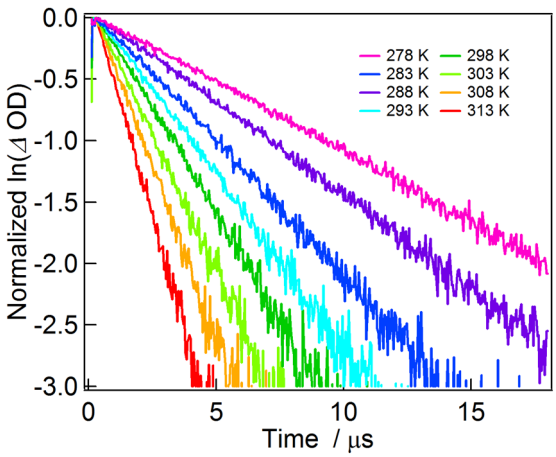

Figure S16. First-order kinetic plots of **1aR** monitored at 710 nm in degassed benzene (3.1×10^{-4} M).

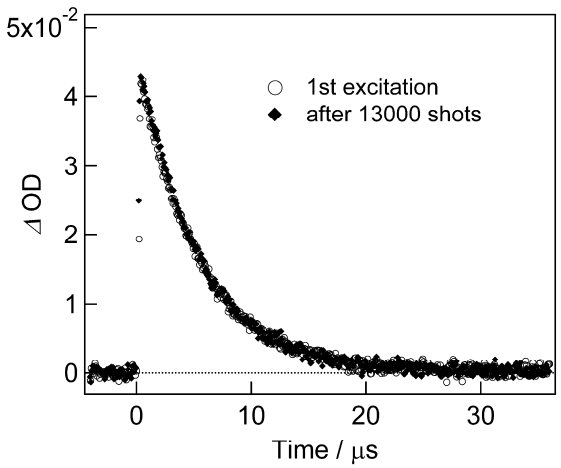

Figure S17. Decay profiles of the transient absorbance at 710 nm of **1aR** in degassed benzene, measured at 298 K (excitation wavelength, 355 nm; pulse width, 5 ns; power, 4 J/pulse).

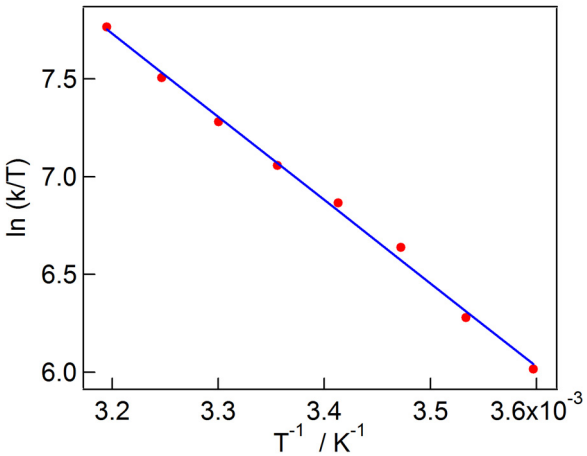

Figure S18. Eyring plots for the thermal back-reaction of **1aR** in degassed benzene solution (3.1×10^{-4} M).

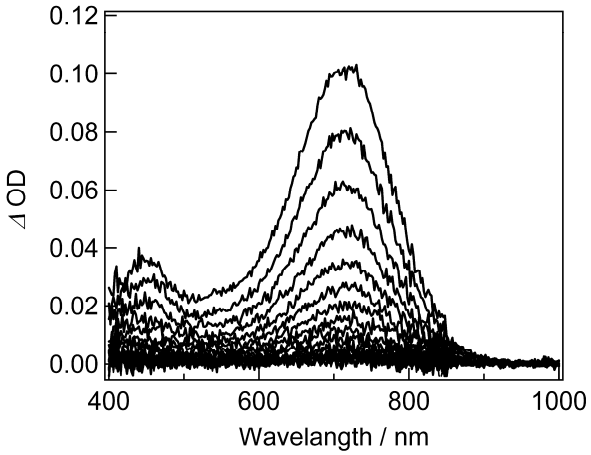

Figure S19. Transient vis-NIR absorption spectra of **1aR** in degassed benzene at 298 K with the time interval of 0.8 μs (3.1×10^{-4} M).

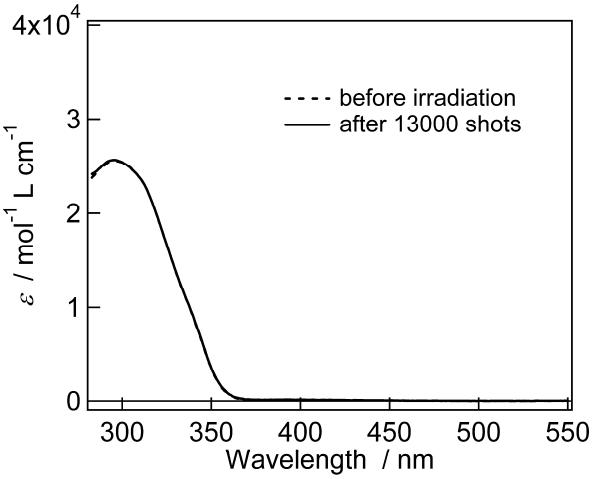

Figure S20. UV–vis absorption spectra of **1a** before (dashed line) and after (solid line) laser pulse irradiation (excitation wavelength, 355 nm; pulse width, 5 ns; power, 4 J/pulse).

Table S4. First-order rate constants for the thermal back-reaction of **1bR**.

T / K	k / s^{-1}
278	1.7×10^{3}
283	2.5×10^{3}
288	3.6×10^{3}
293	5.3×10^{3}
298	6.9×10^{3}
303	9.7×10^{3}
308	1.3×10^{4}
313	1.8×10^{4}

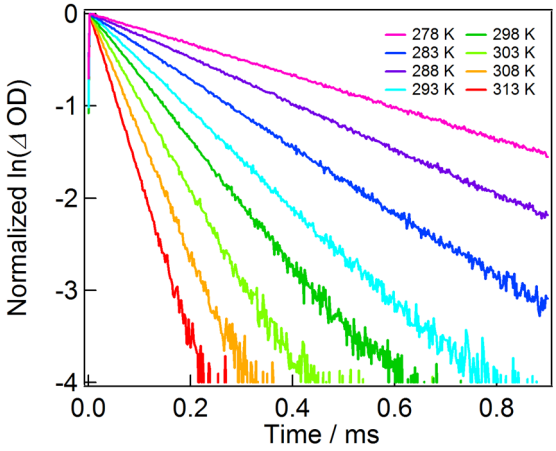

Figure S21. First-order kinetic plots of **1bR** monitored at 710 nm in degassed benzene (2.6×10^{-4} M).

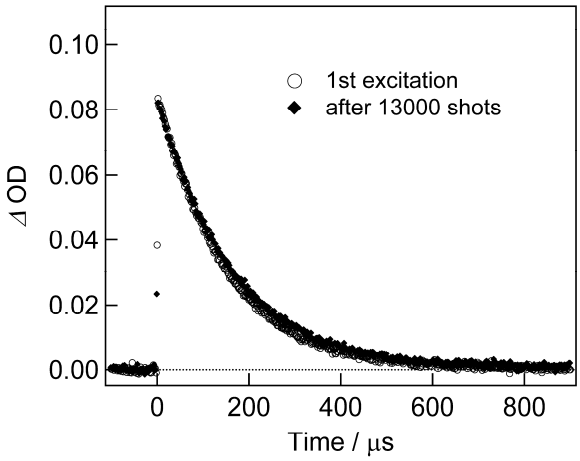

Figure S22. Decay profiles of the transient absorbance at 7100 nm of **1bR** in degassed benzene, measured at 298 K (excitation wavelength, 355 nm; pulse width, 5 ns; power, 4 J/pulse)

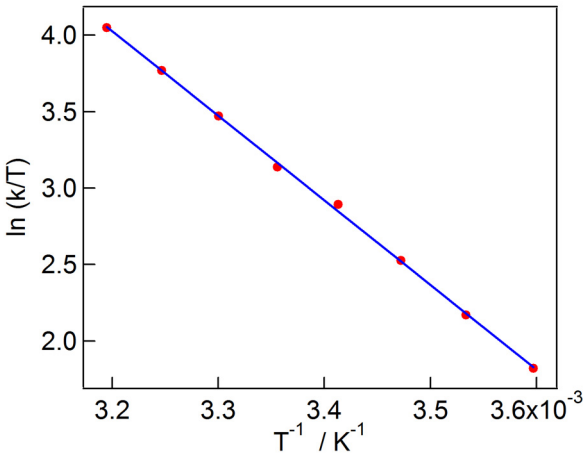

Figure S23. Eyring plots for the thermal back-reaction of **1bR** in degassed benzene solution (2.6×10^{-4} M).

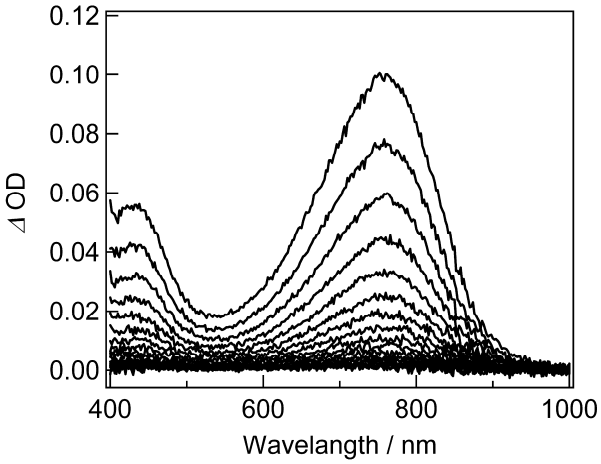

Figure S24. Transient vis-NIR absorption spectra of **1bR** in degassed benzene at 298 K with the time interval of 40 μs (2.6×10^{-4} M).

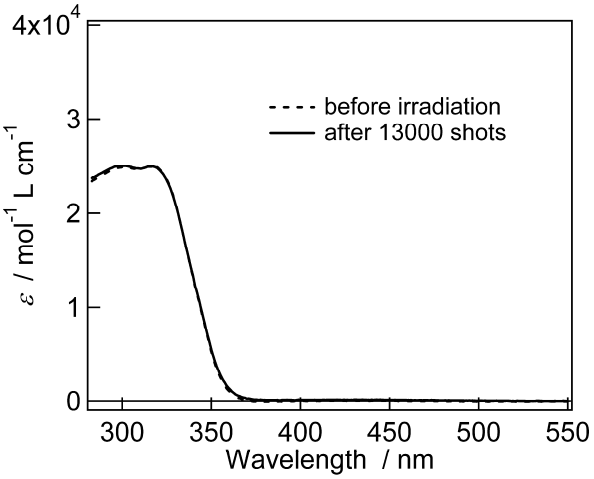

Figure S25. UV–vis absorption spectra of **1b** before (dashed line) and after (solid line) laser pulse irradiation (excitation wavelength, 355 nm; pulse width, 5 ns; power, 4 J/pulse).

Table S5. First-order rate constants for the thermal back-reaction of **1cR**.

T / K	k / s^{-1}
278	5.9×10^{4}
283	8.4×10^{4}
288	1.2×10^{5}
293	1.5×10^{5}
298	1.9×10^{5}
303	2.4×10^{5}
308	3.3×10^{5}
313	4.4×10^{5}

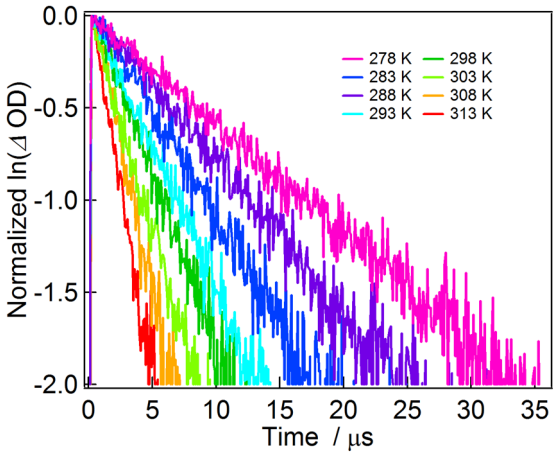

Figure S26. First-order kinetic plots of **1cR** monitored at 710 nm in degassed benzene (3.3×10^{-4} M).

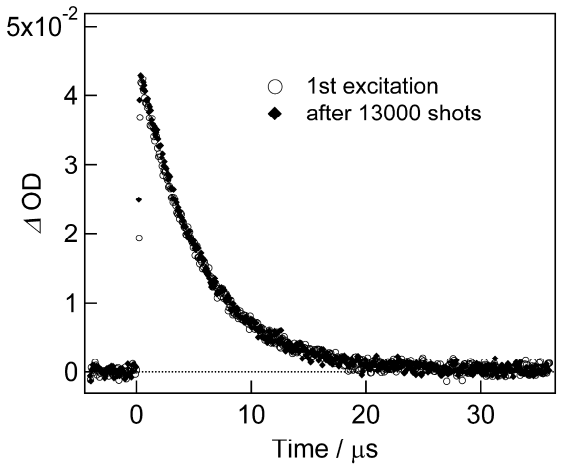

Figure S27. Decay profiles of the transient absorbance at 710 nm of **1cR** in degassed benzene, measured at 298 K (excitation wavelength, 355 nm; pulse width, 5 ns; power, 4 J/pulse)

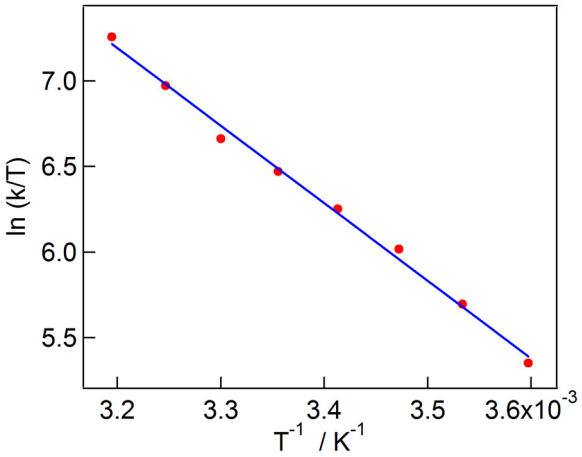

Figure S28. Eyring plots for the thermal back-reaction of **1cR** in degassed benzene solution (2.6×10^{-4} M).

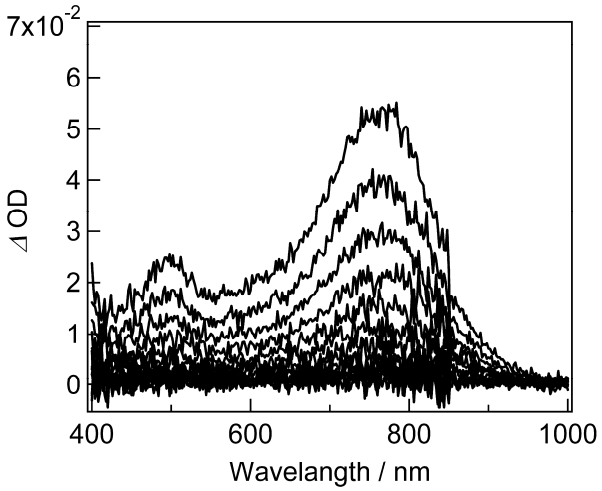

Figure S29. Transient vis-NIR absorption spectra of **1cR** in degassed benzene at 298 K with the time interval of 1.6 μs (2.6×10^{-4} M).

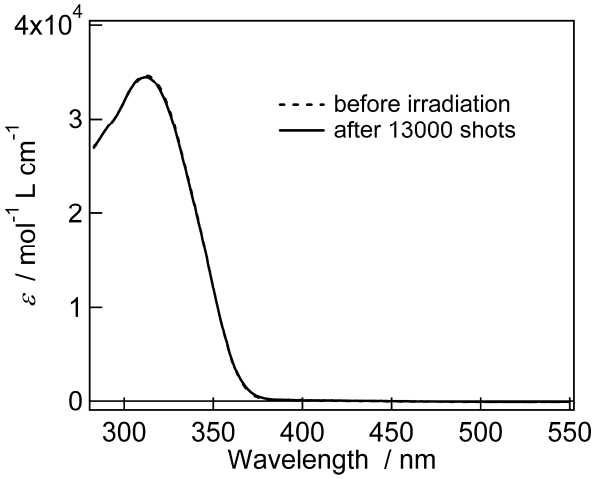

Figure S30. UV–vis absorption spectra of **1c** before (dashed line) and after (solid line) laser pulse irradiation (excitation wavelength, 355 nm; pulse width, 5 ns; power, 4 J/pulse).

8. ESR Spectra

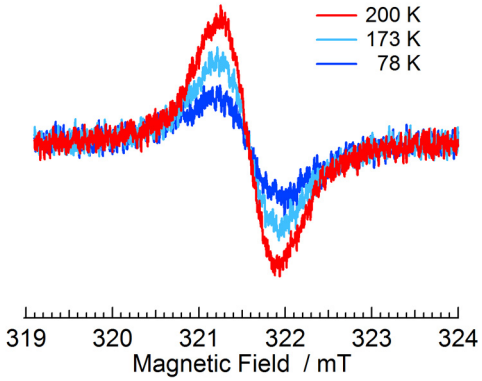

Figure S31. Variable-temperature ESR spectra of **1aR** under UV irradiation in benzene. UV irradiation was carried out using a Keyence UV-400 series UV-LED (UV-50H type), equipped with a UV-L6 lens unit (365 nm, irradiation power 300 mW/cm^2).

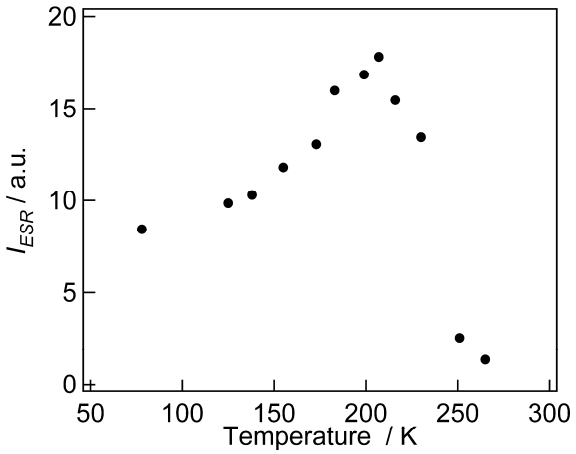

Figure S32. Temperature dependence of the ESR signal intensity of **1aR** generated by UV irradiation in benzene. UV irradiation was carried out using a Keyence UV-400 series UV-LED (UV-50H type), equipped with a UV-L6 lens unit (365 nm, irradiation power 300 mW/cm^2).

9. DFT Calculation

The calculation was carried out using the Gaussian 09 program (Revision D.01).[S4] The molecular structure was fully optimized at the UB3LYP/6-31+G(d,p) level of theory, and analytical second derivative was computed using vibrational analysis to confirm each stationary point to be a minimum.

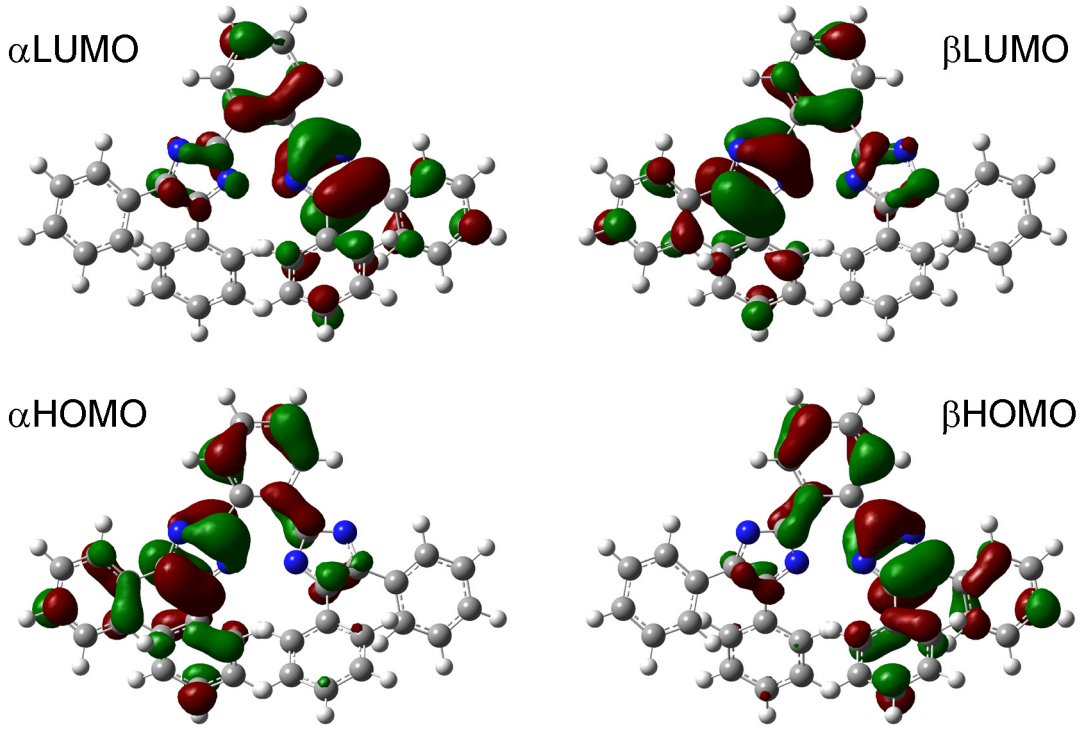

Figure S33. Frontier molecular orbitals of the open-shell singlet state of **1aR** obtained by the broken-symmetry DFT method at the UB3LYP/6-31+G(d,p) level.

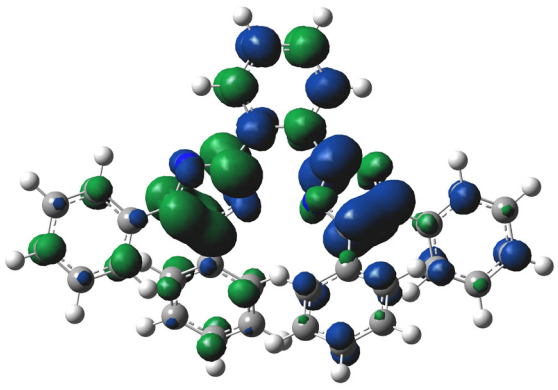

Figure S34. Spin density distributions of the open-shell singlet state of **1aR** (UB3LYP/6-31+G(d,p)).

Table S6. Standard orientation of the optimized geometry for the open-shell singlet state of **1aR**.

Center Number	Atomic Number	Coordinates (Angstroms) X	Y	Z
1	6	-1.3743132	4.2424773	0.2769321
2	6	-0.7142871	3.0010983	0.0820321
3	8	0.7142880	3.0010983	-0.0820319
4	6	1.3743140	4.2424774	-0.2769329
5	6	0.6887280	5.4363825	-0.1591269
6	6	-0.6887272	5.4363825	0.1591271
7	6	-1.5227121	1.8293121	-0.0877609
8	8	1.5227131	1.8293122	0.0877611
9	6	-1.1434381	0.7448021	-0.8452450
10	6	-2.1960121	-0.0574680	-0.8372160
11	6	-3.2503522	0.5719540	0.0028531
12	6	-2.8071762	1.7585321	0.3992521
13	6	2.8071772	1.7585312	-0.3992519
14	6	3.2503523	0.5719532	-0.0028539
15	7	2.1960122	-0.0574689	0.8372162
16	6	1.1434391	0.7448021	0.8452452
17	6	-2.2199071	-1.2798921	-1.6473220
18	6	-4.5545603	0.0655809	0.4357911
19	6	4.5545594	0.0655802	-0.4357929
20	6	2.2199082	-1.2798910	1.6473242
21	7	-3.4010112	-1.7675272	-2.2405471
22	6	-3.3710711	-2.9029063	-3.0503721
23	6	-2.1667110	-3.5753893	-3.2776792
24	6	-0.9853810	-3.0949792	-2.7010651
25	6	-1.0084480	-1.9555031	-1.9009081
26	6	-5.5910874	0.9793330	0.7186051
27	6	-6.8282925	0.5302779	1.1723792
28	6	-7.0519375	-0.8374412	1.3710462
29	6	-6.0263984	-1.7518802	1.1137202
30	6	-4.7895813	-1.3077492	0.6467051
31	6	4.7895804	-1.3077499	-0.6467100
32	6	6.0263966	-1.7518819	-1.1137270
33	6	7.0519356	-0.8374428	-1.3710520
34	6	6.8282916	0.5302753	-1.1723820
35	6	5.5910874	0.9793313	-0.7186070
36	6	1.0084492	-1.9555021	1.9009092

37	6	0.9853812	-3.0949772	2.7010683
38	6	2.1667103	-3.5753862	3.2776853
39	6	3.3710704	-2.9029021	3.0503783
40	6	3.4010113	-1.7675240	2.2405523
41	6	-2.4431213	4.2254013	0.4568261
42	1	2.4431221	4.2254014	-0.4568259
43	1	1.2164670	6.3777835	-0.2801329
44	1	-1.2164652	6.3777835	0.2801321
45	1	-4.3382443	-1.2435642	-2.0893941
46	1	-4.2887972	-3.2582873	-3.5100022
47	1	-2.1470540	-4.4621184	-3.9047012
48	1	-0.0449929	-3.6087822	-2.8786071
49	1	-0.0962029	-1.5680581	-1.4610110
50	1	-5.4043484	2.0379051	0.5747811
51	1	-7.6198436	1.2457919	1.3755312
52	1	-8.0162355	-1.1862223	1.7291962
53	1	-6.1872934	-2.8127513	1.2819862
54	1	-3.9961172	-2.0245302	0.4669911
55	1	3.9961154	-2.0245300	-0.4669969
56	1	6.1872896	-2.8127530	-1.2819950
57	1	8.0162337	-1.1862238	-1.7292030
58	1	7.6198436	1.2457893	-1.3755330
59	1	5.4043494	2.0379033	-0.5747800
60	1	0.0962041	-1.5680591	1.4610112
61	1	0.0449931	-3.6087812	2.8786093
62	1	2.1470533	-4.4621132	3.9047084
63	1	4.2887964	-3.2582821	3.5100114
64	1	4.3382434	-1.2435609	2.0894002

SCF Done: E(RB3LYP) = -1697.71466261 A.U.

Zero-point correction= 0.500318 (Hartree/Particle)

Thermal correction to Energy= 0.531058

Thermal correction to Enthalpy= 0.532002

Thermal correction to Gibbs Free Energy= 0.434574

Sum of electronic and zero-point Energies= -1604.857330

Sum of electronic and thermal Energies= -1604.826590

Sum of electronic and thermal Enthalpies= -1604.825646

Sum of electronic and thermal Free Energies= -1604.923074

Low frequencies --- -0.6752 -0.0081 -0.0068 -0.0047 2.2456 2.9779

Low frequencies --- 13.4202 15.1781 20.6712

10. TDDFT Calculation

Time-dependent DFT (TDDFT) calculation was performed to assign the transient absorption spectra of **1aR** at the B3LYP/6-31+G(d,p) level of the theory. Excitation energies and oscillator strength, calculated vis–NIR absorption spectra are summarized in Figure S35 and Table S6.

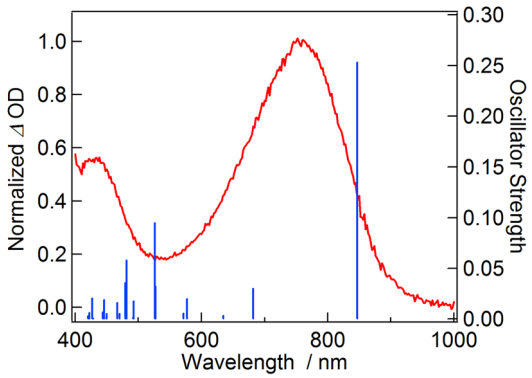

Figure S35. Vis–NIR transient absorption spectrum in benzene and the calculated spectrum by the TDDFT method for **1aR**. The calculated spectra (UB3LYP/6-31+G(d,p)) are shown by the vertical blue lines.

Table S7. Excitation energies and oscillator strengths of **1aR**.

	Excited State		Wavelength/nm	Oscillator Strength
1	αHOMO → αLUMO	0.70819	1478.94	0.0003
	βHOMO → βLUMO	0.70819		
2	αHOMO → αLUMO	-0.70415	846.80	0.2530
	βHOMO → βLUMO	0.70415		
3	αHOMO−2 → αLUMO	-0.14253	681.85	0.0300
	αHOMO−1 → αLUMO	-0.65380		
	βHOMO−2 → βLUMO	0.14253		
	βHOMO−2 → βLUMO	0.65380		

11. CASSCF Calculation

CASSCF(8,8)/6-31G(d)//B3LYP/6-31+G(d,p) calculation was performed to obtain the singlet biradical index *y* of **1aR** from the LUMO occupation number. The initial guess was calculated at HF/6-31(d) level.

Final one electron symbolic density matrix:

	1	2	3	4	5
1	0.196153D+01				
2	0.117014D-08	0.193123D+01			
3	0.181382D-06	-0.270610D-06	0.196173D+01		
4	-0.440557D-06	0.131525D-08	-0.104291D-08	0.171619D+01	
5	0.206706D-08	-0.917431D-06	0.253916D-05	0.237881D-08	0.286143D+00
6	-0.376912D-05	0.147799D-08	-0.297377D-08	0.151832D-05	-0.163993D-08
7	-0.388395D-05	0.464208D-08	0.555987D-08	-0.125389D-05	-0.334509D-08
9	0.627813D-08	-0.257553D-05	-0.108245D-05	-0.209527D-08	0.977708D-06

	6	7	8
6	0.659511D-01		
7	0.965025D-06	0.386674D-01	
8	-0.157557D-09	0.826036D-06	0.385577D-01

12. Reference

S1. Che, C.; Li, S.; Yu, Z.; Li, F.; Xin, S.; Zhou, L.; Lin, S.; Yang, Z. *ACS Comb. Sci.* **2013**, *15*, 202.

S2. Sheldrick GM. *SHELXS-97* and *SHELXL-97*; University of Gottingen, Germany, 1997.

S3. Sheldrick GM. *SADABS*; University of Gottingen, Germany, 1996.

S4. Frisch, M. J.; Trucks, G. W.; Schlegel, H. B.; Scuseria, G. E.; Robb, M. A.; Cheeseman, J. R.; Scalmani, G.; Barone, V.; Mennucci, B.; Petersson, G. A.; Nakatsuji, H.; Caricato, M.; Li, X.; Hratchian, H. P.; Izmaylov, A. F.; Bloino, J.; Zheng, G.; Sonnenberg, J. L.; Hada, M.; Ehara, M.; Toyota, K.; Fukuda, R.; Hasegawa, J.; Ishida, M.; Nakajima, T.; Honda, Y.; Kitao, O.; Nakai, H.; Vreven, T.; Montgomery, J. A., Jr.; Peralta, J. E.; Ogliaro, F.; Bearpark, M.; Heyd, J. J.; Brothers, E.; Kudin, K. N.; Staroverov, V. N.; Kobayashi, R.; Normand, J.; Raghavachari, K.; Rendell, A.; Burant, J. C.; Iyengar, S. S.; Tomasi, J.; Cossi, M.; Rega, N.; Millam, N. J.; Klene, M.; Knox, J. E.; Cross, J. B.; Bakken, V.; Adamo, C.; Jaramillo, J.; Gomperts, R.; Stratmann, R. E.; Yazyev, O.; Austin, A. J.; Cammi, R.; Pomelli, C.; Ochterski, J. W.; Martin, R. L.; Morokuma, K.; Zakrzewski, V. G.; Voth, G. A.; Salvador, P.; Dannenberg, J. J.; S. 50 Dapprich, S.; Daniels, A. D.; Farkas, Ö.; Foresman, J. B.; Ortiz, J. V.; Cioslowski, J.; Fox, D. J. Gaussian 09, Revision D.01; Gaussian, Inc.: Wallingford CT, 2009.